X-ray phase imaging with a grating interferometer

Timm Weitkamp, Ana Diaz and Christian David

Laboratory for Micro- and Nanotechnology, Paul Scherrer Institut, 5232 Villigen PSI, Switzerland

timm.weitkamp@psi.ch

Franz Pfeiffer and Marco Stampanoni

Swiss Light Source, Paul Scherrer Institut, 5232 Villigen PSI, Switzerland

Peter Cloetens and Eric Ziegler

European Synchrotron Radiation Facility, B. P. 220, 38043 Grenoble Cedex, France

Abstract: Using a high-efficiency grating interferometer for hard X rays (10–30 keV) and a phase-stepping technique, separate radiographs of the phase and absorption profiles of bulk samples can be obtained from a single set of measurements. Tomographic reconstruction yields quantitative three-dimensional maps of the X-ray refractive index, with a spatial resolution down to a few microns. The method is mechanically robust, requires little spatial coherence and monochromaticity, and can be scaled up to large fields of view, with a detector of correspondingly moderate spatial resolution. These are important prerequisites for use with laboratory X-ray sources.

OCIS codes: (340.7450) X-ray interferometry; (340.7440) X-ray imaging; (170.6960) Tomography

References and links

1. R. Fitzgerald, "Phase-Sensitive X-Ray Imaging," Phys. Today **53**(7), 23–27 (2000).
2. A. Momose, "Phase-sensitive imaging and phase tomography using X-ray interferometers," Opt. Express **11**, 2303–2314 (2003). URL http://www.opticsexpress.org/abstract.cfm?URI=OPEX-11-19-2303.
3. U. Bonse and M. Hart, "An X-ray interferometer," Appl. Phys. Lett. **6**, 155–156 (1965).
4. A. Momose, T. Takeda, Y. Itai, and K. Hirano, "Phase-contrast X-ray computed tomography for observing biological soft tissues," Nature Med. **2**, 473–475 (1996).
5. F. Beckmann, U. Bonse, F. Busch, and O. Günnewig, "X-ray Microtomography Using Phase Contrast for the Investigation of Organic Matter," J. Comp. Assist. Tomography **21**, 539–553 (1997).
6. V. N. Ingal and E. A. Beliaevskaya, "X-ray plane-wave topography observation of the phase contrast from a non-crystalline object," J. Phys. D **28**, 2314–2317 (1995).
7. T. J. Davis, D. Gao, T. E. Gureyev, A. W. Stevenson, and S. W. Wilkins, "Phase-contrast imaging of weakly absorbing materials using hard X-rays," Nature (London) **373**, 595–598 (1995).
8. D. Chapman, W. Thomlinson, R. E. Johnston, D. Washburn, E. Pisano, N. Gmür, Z. Zhong, R. Menk, F. Arfelli, and D. Sayers, "Diffraction enhanced x-ray imaging," Phys. Med. Biol. **42**, 2015–2025 (1997).
9. A. Snigirev, I. Snigireva, V. Kohn, S. Kuznetsov, and I. Schelokov, "On the possibilities of x-ray phase contrast microimaging by coherent high-energy synchrotron radiation," Rev. Sci. Instr. **66**, 5486–5492 (1995).
10. S. W. Wilkins, T. E. Gureyev, D. Gao, A. Pogany, and A. W. Stevenson, "Phase-contrast imaging using polychromatic hard X-rays," Nature (London) **384**, 335–337 (1996).
11. P. Cloetens, W. Ludwig, J. Baruchel, D. V. Dyck, J. V. Landuyt, J. P. Guigay, and M. Schlenker, "Holotomography: Quantitative phase tomography with micrometer resolution using hard synchrotron radiation x rays," Appl. Phys. Lett. **75**, 2912–2914 (1999).

#7950 - $15.00 US Received 27 June 2005; revised 1 August 2005; accepted 1 August 2005

12. C. David, B. Nöhammer, H. H. Solak, and E. Ziegler, "Differential x-ray phase contrast imaging using a shearing interferometer," Appl. Phys. Lett. **81**, 3287–3289 (2002).
13. A. Momose, "Demonstration of X-Ray Talbot Interferometry," Jpn. J. Appl. Phys. **42**, L866–L868 (2003).
14. T. Weitkamp, B. Nöhammer, A. Diaz, C. David, and E. Ziegler, "X-ray wavefront analysis and optics characterization with a grating interferometer," Appl. Phys. Lett. **86**, 054,101 (2005).
15. If the incoming wave is not plane but curved, with a radius of curvature R, the only additional consideration that must be made is that the interference fringe period at a distance z downstream of the grating scales with a factor of $M = 1 + z/R$..
16. K. Creath, "Phase-measurement Interferometry Techniques," in *Progress In Optics XXVI*, E. Wolf, ed., pp. 349–393 (Elsevier Science, 1988).
17. M. Born and E. Wolf, *Principles of Optics*, sixth ed. (Pergamon Press, Oxford, England, 1993).
18. It is conceivable to measure the derivatives of Φ along both transverse directions x and y instead of only one as described in this paper. This may make phase reconstruction more robust in the presence of phase wrapping. However, it would require a more complicated measurement procedure and, preferably, two-dimensional gratings, which cannot be fabricated with high aspect ratios using the same technology as for the line gratings.
19. B. F. McEwen, K. H. Downing, and R. M. Glaeser, "The relevance of dose-fractionation in tomography of radiation-sensitive specimens," Ultramicroscopy **60**, 357–373 (1995).
20. The energy spectrum was obtained by filtering the continuous spectrum from a wiggler source with a combination of absorption foils (Zr 0.1 mm, Si 0.8 mm) and the energy-dependent efficiency of the detector scintillator, a 20-μm-thick yttrium aluminium garnet (YAG) crystal.
21. For example, the two K_α lines in the emission spectrum of a molybdenum target are 0.1 keV apart from each other, at a mean energy of 17.4 keV.
22. T. Weitkamp, "XWFP: An X-ray wavefront propagation software package for the IDL computer language," in *Advances in Computational Methods for X-Ray and Neutron Optics*, M. Sanchez del Rio, ed., vol. 5536 of *Proc. SPIE*, pp. 181–189 (2004).

1. Introduction

X-ray radiographic absorption imaging is an invaluable standard tool in medical diagnostics and is increasingly used in other research areas such as environmental and materials science. For such important classes of samples as biological tissue, polymers, and fiber composites, however, the use of conventional X-ray radiography is limited because these objects show only weak absorption.

However, the cross section for elastic scattering of hard X rays in matter, which causes a phase shift of the wave passing through the object of interest, is usually much greater than that for absorption. For example, 17.5-keV X rays that pass through a 50-μm-thick sheet of biological tissue are attenuated by only a fraction of a percent, while the phase shift is close to π.

Recording the X-ray phase shift rather than only the absorption thus has the potential of substantially increased contrast. Consequently, various phase-sensitive X-ray imaging methods were developed in the past years [1, 2]. They can be classified into interferometric methods [3, 4, 5], techniques using an analyzer crystal [6, 7, 8], and free-space propagation methods [9, 10, 11]. These techniques differ vastly in the nature of the signal recorded, the experimental setup, and the requirements on the illuminating radiation (especially its spatial coherence and monochromaticity). Although some of them yield excellent results for specific problems, none is very widely used. In particular, none of them has so far found application in medical diagnostics, where the spatial resolution needed is moderate compared to current technological limits in synchrotron-based methods, but which requires a large field of view of many centimeters, the efficient use of broadband ($\gtrsim 1\%$) radiation as provided by laboratory X-ray generators, and a reasonably compact setup.

2. Grating interferometer

The use of gratings as optical elements in hard X-ray phase imaging can overcome problems that so far impair the wider use of phase contrast in X-ray radiography and tomography. First

#7950 - $15.00 US Received 27 June 2005; revised 1 August 2005; accepted 1 August 2005

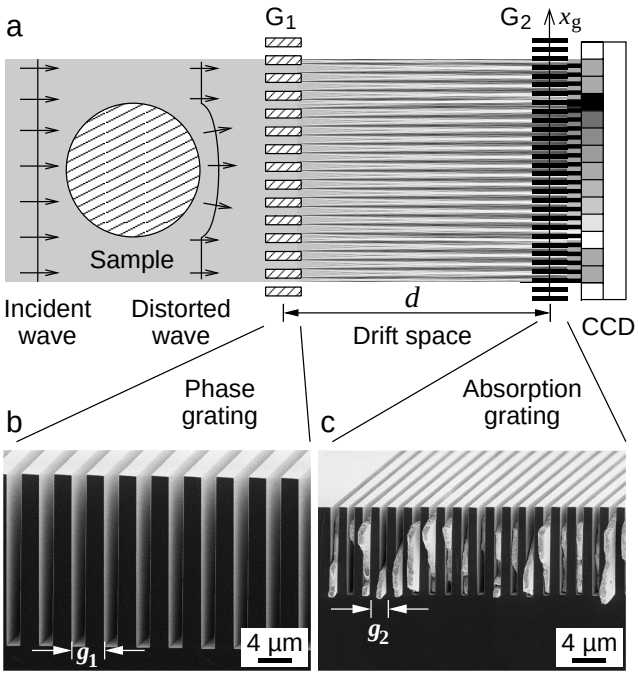

Fig. 1. Grating-based hard X-ray interferometer. (a) Principle: the beam splitter grating (G1) splits the incident beam into essentially two diffraction orders, which form a periodic interference pattern in the plane of the analyzer grating. A phase object in the incident beam will cause slight refraction, which results in changes of the locally transmitted intensity through the analyzer. (b,c) Scanning electron micrographs of cross sections through the gratings used. The silicon beam-splitter grating (b) has a pitch of 4 μm, i.e., twice that of the analyzer grating (c), which was made by filling the grooves of a silicon grating with gold by electroplating.

experiments with X-ray grating interferometers were reported recently [12, 13, 14]. Here we demonstrate quantitative two- and three-dimensional phase reconstruction with radiation of a bandwidth up to 5%, using highly efficient gratings.

The interferometer consists of a phase grating G_1 (i.e., a grating whose lines show negligible absorption but substantial phase shift) and an absorption grating G_2 (Fig. 1). The first grating acts as a beam splitter and divides the incoming beam essentially into the two first diffraction orders. Since the wavelength λ of the illuminating hard X rays ($\approx 10^{-10}$ m) is much smaller than the grating pitch ($\approx 10^{-6}$ m), the angle between the two diffracted beams is so small that they overlap almost completely. Downstream of the beam-splitter grating, the diffracted beams interfere and, when illuminated with a plane or spherical wave, form linear periodic fringe patterns in planes perpendicular to the optical axis. For a phase grating with a phase shift of π illuminated by a plane wave, the periodicity g of the fringe pattern equals half the period of G_1 [15]. Neither the period nor the lateral position of these fringes depends on the wavelength of the radiation used. Perturbations of the incident wave front, such as those induced by refraction on an object in the beam, lead to local displacement of the fringes (Fig. 1). The fundamental idea of the method presented here is to detect the positions of the fringes and determine from these the shape of the wave front. However, since the pitch of the phase grating (and thus the spacing of the interference fringes) does not exceed a few microns, an area detector placed in the detection plane will generally not have sufficient resolution to resolve the fringes, let

#7950 - $15.00 US Received 27 June 2005; revised 1 August 2005; accepted 1 August 2005

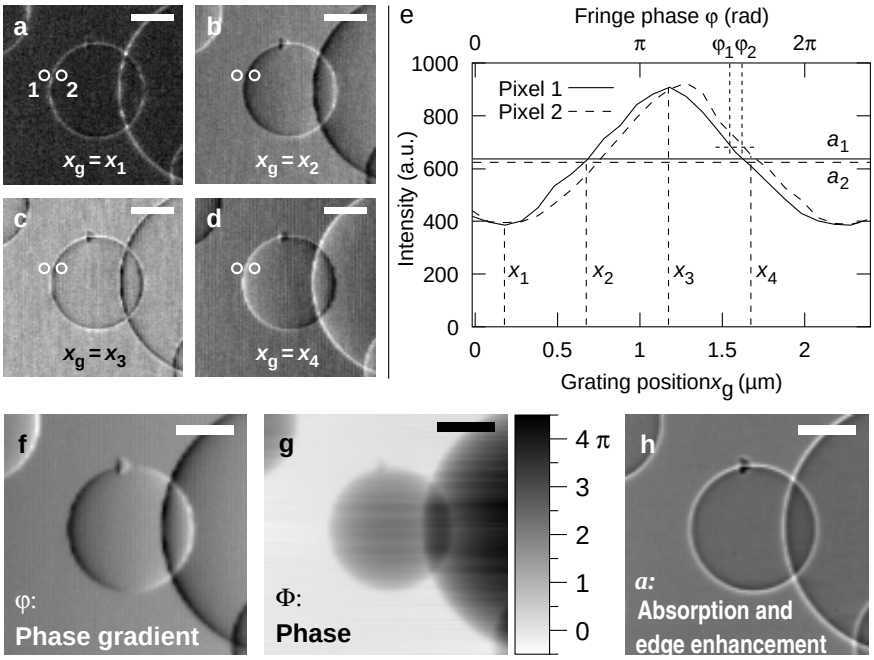

Fig. 2. Principle of phase stepping. (a-d) Interferograms of polystyrene spheres (100 and 200 μm diameter), taken at the different relative positions $x_g = x_1, \ldots, x_4$ of the two interferometer gratings. (e) Intensity oscillation in two different detector pixels $i = 1,2$ as a function of x_g. For each pixel, the oscillation phase φ_i and the average intensity a_i over one grating period can be determined. (f) Image of the oscillation phase φ for all pixels. (g) Wave-front phase Φ retrieved from φ by integration. (h) Image of the averaged intensity a for all pixels, equivalent to a non-interferometric image. The length of the scale bar is 50 μm.

alone the exact position of their maxima. Therefore, a grating G_2 with absorbing lines and the same periodicity and orientation as the fringes is placed in the detection plane, immediately in front of the detector. This analyzer grating acts as a transmission mask for the detector and transforms local fringe position into signal intensity variation. The detected signal profile thus contains quantitative information about the phase gradient of the object.

3. Phase stepping

To separate this phase information from other contributions to the signal, such as absorption in the sample, inhomogeneous illumination or imperfections of the gratings, the phase-stepping approach used in visible-light interferometry [16] was adapted to this setup. One of the gratings is scanned along the transverse direction x_g (cf. Fig. 1) over one period of the grating, and for every point of the scan an image is taken, as shown in Fig. 2(a-d). The intensity signal $I(x,y)$ in each pixel (x,y) in the detector plane oscillates as a function of x_g [Fig. 2(e)]. The phases $\varphi(x,y)$ of the intensity oscillations in each pixel [Fig. 2(f)] are related to the wave-front phase profile Φ(x,y), the X-ray wavelength λ, the distance d between the two gratings, and the period g_2 of the absorption grating by [17]

$$\varphi = \frac{\lambda d}{g_2} \frac{\partial \Phi}{\partial x}. \qquad (1)$$

#7950 - $15.00 US
Received 27 June 2005; revised 1 August 2005; accepted 1 August 2005

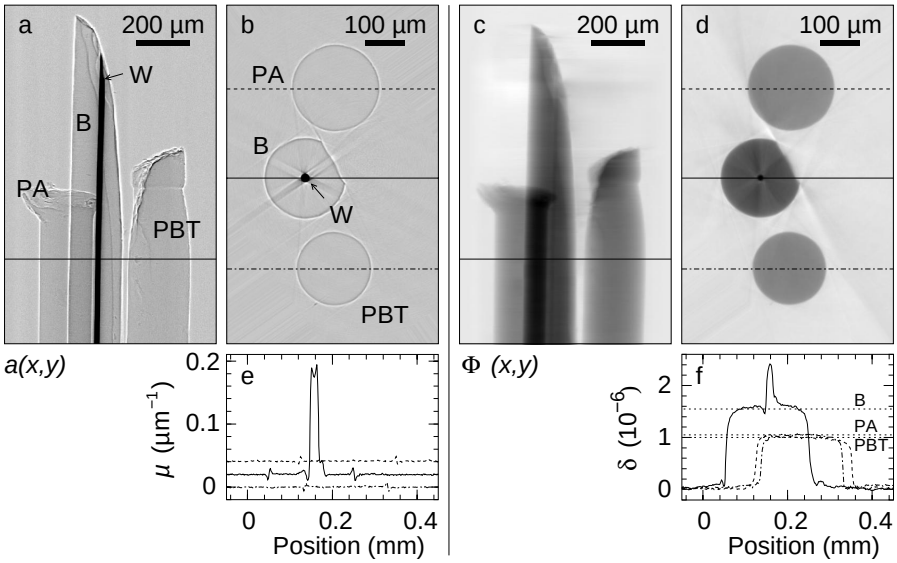

Fig. 3. Radiographs and tomograms of a reference sample consisting of two polymer fibers (polyamide, PA, and polybutylene terephthalate, PBT) and a boron fiber with a tungsten core, acquired with broadband radiation of (17.5 ± 0.5) keV photon energy. (a) Non-interferometric projection image. (b) Tomographic slice, corresponding to the position indicated by the horizontal line in (a). (c) Reconstructed phase projection. (d) Tomographic slice through the refractive-index distribution. (e,f) Section profiles through the fiber centers in, respectively, the non-interferometric tomogram (e) and the phase tomogram (f) (solid: B/W, dashed: PA, dash-dotted: PBT, dotted: literature values). In (e), the lines for PA and B/W are displaced along the ordinate axis for clarity.

φ contains no other contributions, particularly no absorption contrast. The phase profile of the object can thus be retrieved from $\varphi(x,y)$ by a simple one-dimensional integration, as shown in Fig. 2(g). In the general case in which the wave front incident on the object already shows some distortion, the background phase distribution $\Phi_{\mathrm{back}}(x,y)$ should be measured (with the object removed from the beam) and then subtracted. Even where the range of phase values exceeds 2π, such as in the example in Fig. 2(g), phase unwrapping is generally not necessary because the measured quantity φ, essentially the first derivative of Φ (Eq. 1), will not exceed π as long as the phase gradients in the sample are not too steep [18].

The minimum number of steps for a phase-stepping scan that allows to extract φ is three in the case of a sinusoidal intensity oscillation; the results shown here were obtained with eight phase steps per projection. The results indicate that an effect comparable to dose fractionation [19] in tomography occurs, i. e., even a series of phase-stepping interferograms with poor pixel statistics in each frame can yield a processed phase-gradient image with sufficient statistics. An investigation of this effect goes beyond the scope of this paper.

4. Tomographic reconstruction

Tomographic reconstruction of $\Phi(x,y)$ taken for a sufficient number of different viewing angles of the sample yields the three-dimensional distribution of the X-ray refractive index $n(x',y',z')$ of the object. Given the small deviation of n from unity, the refractive index is generally expressed in terms of its decrement $\delta(x',y',z') = 1 - n$.

Another quantity contained in the data from a phase-stepping scan is the average signal

#7950 - $15.00 US Received 27 June 2005; revised 1 August 2005; accepted 1 August 2005

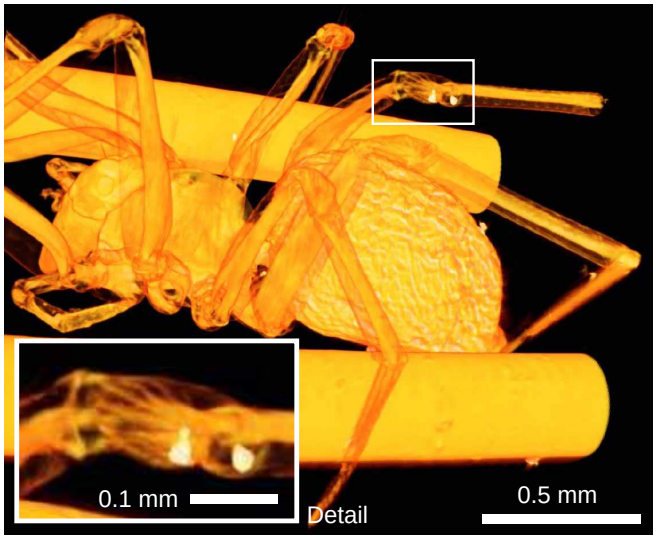

Fig. 4. Three-dimensional density-projection rendering of the reconstructed refractive index of a small spider, supported by two polyamide fibers. These data were taken at a photon energy of 14.4 keV with gratings of pitch $g_1 = 4\,\mu$m, $g_2 = 2\,\mu$m, and an intergrating distance of $d = 23.2$ mm.

for each pixel over an entire oscillation, $a(x,y)$ [Fig. 2(h)]. It is identical to the transmission radiography signal that would be measured in a radiograph taken without the interferometer. It contains the projected absorption coefficient and, depending on experimental geometry and detector resolution, edge-enhancing Fresnel diffraction contrast. A single phase-stepping scan thus yields both the phase and the absorption image.

Since the position of the interference fringes formed behind the beam-splitter grating is, over a wide range of photon energies, independent of wavelength, the interferometer is largely achromatic and can efficiently be used with polychromatic radiation. Reconstructed phase projections and tomograms will still be quantitative, showing the distribution of the refractive index averaged over the photon-energy band.

Figure 3 shows processed absorption and phase projection images $a(x,y)$ and $\Phi(x,y)$, as well as reconstructed tomograms, of a reference sample made of three fibers with almost identical, very weak absorption (except for the core of the central fiber), but different refractive index. In the phase tomogram [Fig. 3(d)], the different constituents of the fibers can clearly be distinguished by their reconstructed refractive indices δ, while the noninterferometric tomogram [Fig. 3(b)] does not allow discriminating between the materials. Moreover, the values for δ agree well with the literature [Fig. 3(f)], with the only exception of the tungsten core of one of the fibers, whose diameter is at the limit of spatial resolution for quantitatively correct reconstruction. For these measurements, radiation with a mean photon energy of 17.5 keV and a bandwidth of 1 keV was used [20]. This energy width is compatible to that of a set X-ray emission lines in the spectrum of a laboratory source [21]. Phase reconstruction with most other methods would be impaired by the polychromaticity.

A more complex object is shown in Fig. 4. This three-dimensional density-projection rendering of the refractive-index distribution of a small spider reveals details of the internal structure of the animal that would be difficult to access with other techniques. Spatial resolution is a few micrometers.

#7950 - $15.00 US
Received 27 June 2005; revised 1 August 2005; accepted 1 August 2005

5. Design and properties of the interferometer

5.1. Dimensions

The distance d between the two gratings should be chosen to be [17]

$$d_m = \left(m - \frac{1}{2}\right) \frac{g_1^2}{4\lambda}, \quad \text{with} \quad m = 1, 2, 3, \ldots \tag{2}$$

(where g_1 is the pitch of the beam-splitter grating), because at this distance the contrast of the interference fringes has a maximum — a phenomenon related to the Talbot self-imaging effect.

Eq. 2 describes the optimum distance for the case of an illuminating plane wave. For a spherical wave coming from a source at distance L from the beam splitter, the distances rescale so that maximum contrast is achieved at $d'_m = Ld_m/(L - d_m)$.

Eq. 1 implies that the sensitivity of the method increases linearly with the inter-grating distance d. However, the choice of larger d results in a loss of spatial resolution and in larger required transverse coherence length (both on the order of mg_1). If a large field of view is required for a given application, then a detector with correspondingly larger pixels can be used. This is not the case for edge-enhanced non-interferometric imaging, in which the detector must resolve the Fresnel fringes in the image, even if the image resolution needed is inferior to that required for resolving the fringes.

The period g_1 of the beam-splitter grating affects the optimum intergrating distances d_m and the minimum required transverse coherence length l_c, which is $(m-0.5)g_1$. g_1 should therefore be chosen small enough to keep the device compact and operate it efficiently with a source of a given finite size. The lower limit to the grating periods is given by limits in fabrication technology for structures with high aspect ratios (section 5.2) and by the requirements on mechanical stability (section 5.5).

As mentioned above, the period g_2 of the analyzer grating should, for practical purposes, match the period g of the unperturbed interference fringes. For a plane wave, $g_2 = g_1/2$. For a spherical wave with radius L, this rescales to $g_2 = (g_1/2) \times L/(L-d)$. But these conditions do not have to be strictly met. A deviation of g_2 from them will result in moiré fringes in the raw interferograms. If a background phase image is subtracted from the object image, the effects of the moiré fringes cancel out.

5.2. Efficiency, fabrication of gratings

The efficiency of the setup is determined by the efficiencies of the two gratings. The beam-splitter grating lines should ideally induce a phase shift of π and have a duty cycle of 0.5, so that no undiffracted portion, or zeroth order, of the beam is left. In this case, 80% of the incoming intensity are diffracted into the positive and negative first orders, which are used to generate the signal. (The remaining 20 percent go into higher orders, inevitable for a box-profile grating structure.) The absorption contrast of the analyzer grating should be as high as possible. This requires deep structures for both gratings. For an ideal absorption grating, with a duty cycle of 0.5 and total absorption in the grating lines, the efficiency in terms of the fraction of intensity hitting the grating that contributes to the detected signal is 50%.

The gratings shown in Fig. 1(b,c), which largely fulfill these requirements, were made with a production process involving electron-beam lithography, deep etching into silicon [12] and, for the absorption grating, subsequent electroplating of gold. The intensity of the zeroth order of the beam-splitter grating, ideally non-existent, was measured to be less than 5% of the first-order intensity [12]. The absorption of the analyzer grating ($\approx 10\,\mu$m of gold) ranges between 75 and 90% for the photon energies used here. The size of the gratings used in the measurements was a few millimeters in each dimension, but much larger gratings (many cm in each dimension) can be made using photolithography instead of electron-beam lithography.

#7950 - $15.00 US Received 27 June 2005; revised 1 August 2005; accepted 1 August 2005

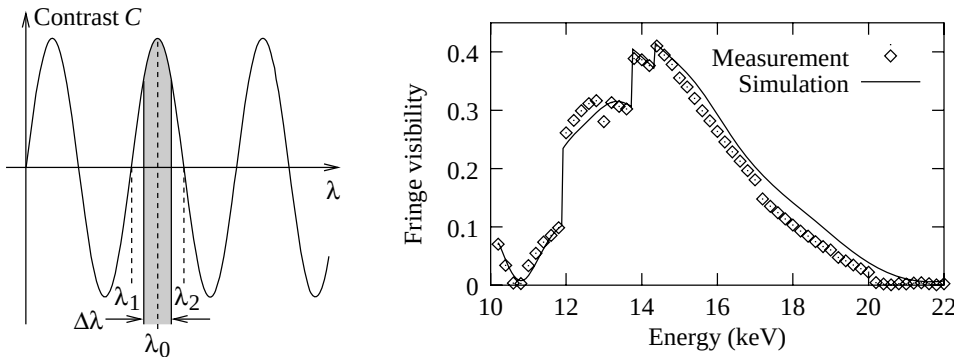

Fig. 5. Left: Contrast transfer for fixed grating periods and intergrating distance as a function of wavelength λ, for ideal gratings. The half-width $\Delta\lambda$ between zero-contrast wavelengths λ_1, λ_2 around the design wavelength λ_0 is a measure of the efficient energy range for a given setup. Right: Measured and simulated efficiency of a grating interferometer, taking into account variations of grating efficiency with photon energy. Here, a photon energy of 14.4 keV was used with an interferometer with grating periods of $g_1 = 4\,\mu$m and $g_2 = 2\,\mu$m, at an intergrating distance of $d = 69.7$ mm. The simulation was made using the XWFP computer code [22].

5.3. Limits of achromaticity

It was mentioned in the previous section that the device is largely achromatic. Set aside any dispersion in the sample, the limits of achromaticity are given by the decrease in efficiency of the interferometer as the X-ray photon energy deviates from the design energy. This efficiency decrease is influenced by three effects. Firstly, the Talbot condition (Eq. 2) is not met for wavelengths other than the design wavelength. The Talbot effect makes that contrast C varies sinusoidally with wavelength, $C \propto \sin(\pi\lambda d/g_2^2)$. The half-width $\Delta\lambda = (\lambda_2 - \lambda_1)/2$ between those wavelengths λ_1 and λ_2 (to either side of the design wavelength λ_0) at which contrast goes through zero can be taken as an effective energy range over which the interferometer operates efficiently (Fig. 5, left). It can be shown easily from the relationships above and Eq. 2 that

$$\Delta\lambda = \frac{\lambda_0}{2m-1}\,. \tag{3}$$

Thus, the higher the order m of the Talbot distance used, the stricter the requirements on monochromaticity. Still, even for the 5th-order Talbot distance, the acceptable bandwidth $\Delta\lambda/\lambda_0$ is more than 10%.

The other two factors affecting the efficiency as the photon energy deviates from its design value are the changes in efficiency of the beam splitter and the analyzer grating. A measurement of all three effects was carried out on a bending-magnet synchrotron beamline by scanning the photon energy selected by a silicon double-crystal monochromator and measuring the visibility of moiré fringes. The results were compared with simulation (Fig. 5, right). They agree well and show an effective bandwidth of 2 keV, for a design energy of 14.4 keV.

5.4. Resolution limit

The spatial resolution of the images obtained with the interferometer is limited (a) as in other imaging systems, by the resolution of the detector, (b) by the fact that the resolution cannot be better than two periods g_2 of the analyzer grating, and (c) by the lateral shear of the two waves created by the beam splitter that interfere in the plane of the analyzer grating. The shear is equal

#7950 - $15.00 US Received 27 June 2005; revised 1 August 2005; accepted 1 August 2005

to the product of the intergrating distance d and the angle between the propagation directions of the two waves, which is $4\lambda/g_1$ if the beam splitter is a phase grating with a phase shift of π in the lines of the grating. Assuming that d is chosen to be a Talbot distance d_m as defined by Eq. 2, then the resulting lateral shear for a Talbot order m is $(m-0.5)g_1 = (2m-1)g_2$.

5.5. Stability and alignment

The issue of stability, alignment, and precision of movement concerns mostly the relative positions of the two gratings. These should be mechanically stable with respect to one another down to lengthscales of approximately one-tenth of the grating period g_2. In the examples shown here, where $g_2 = 2\,\mu$m, this means that stability to 100 nm is largely sufficient. With dimensions of a few centimeters for the entire device, this condition is easily fulfilled. The same lengthscale applies to the precision of the transverse grating motion used in phase stepping, so that a conventional ball-bearing linear stage can be used. Also, thermally-induced or other mechanical drift is not an issue.

The only relevant angular alignment parameter is the relative angle α of the two gratings about the optical axis, i. e., the deviation from parallelism of the lines of one grating with respect to the lines of the other. If this angle is nonzero, the raw interferograms will show moiré fringes [14], the density of which increases with α. A complete suppression of these fringes is achieved if $|\alpha| < g_2/X$, where X is the width of the field of view in the direction along the grating lines. Even if this condition is not met, the effects of moiré fringes in the image will again cancel out in the subtraction of the background phase image. The alignment of α is thus not critical.

6. Conclusion

Experimental results and theoretical considerations show that a grating interferometer can be used for qualitative or quantitative two- and three-dimensional X-ray phase radiography. The use of phase stepping, in which a small number of raw interferograms for each projection radiograph is taken, presents a method to separate absorption from phase signal and to easily retrieve the projected phase, while preserving the resolution of the imaging system.

The moderate requirements on coherence and monochromaticity, the possibility to make large gratings of high quality and efficiency, and the easy alignment and low sensitivity of the setup to mechanical drift suggest that hard X-ray phase imaging with grating interferometers can find application in areas where phase imaging would be desirable, but is currently not widely used.

In particular, the possibility to combine the instrument with imaging systems of a large field of view and the efficient use of broadband sources let us envisage applications in such fields as medical and biological imaging or research on organic materials. Even neutron phase radiography with grating interferometers is conceivable. The dimensions of the gratings needed would be similar to the X-ray case.

Acknowledgments

Data collection for this work was performed at the Swiss Light Source, Paul Scherrer Institut, Villigen, Switzerland, and at the European Synchrotron Radiation Facility (ESRF) in Grenoble, France. We gratefully acknowledge the assistance of A. Grošo and O. Bunk (PSI) and J. Patommel (RWTH Aachen, Germany) during measurements. B. Nöhammer (PSI, now Infineon, Villach, Austria) is acknowledged for fruitful discussions. Part of this work was funded by the Swiss National Science Foundation.

#7950 - $15.00 US Received 27 June 2005; revised 1 August 2005; accepted 1 August 2005